Floodplain Backwater Effect on Overtopping Induced Fluvial Dike Failure

ISMAIL RIFAI, Ph.D. Student, (orcid.org/0000-0002-9840-3697), *EDF R&D, National Laboratory for Hydraulics and Environment, Saint Venant Laboratory for Hydraulics, Chatou, France , and ArGEnCo Department, Research Group Hydraulics in Environmental and Civil Engineering (HECE), University of Liège, Liège, Belgium,*
Email: I.Rifai@doct.ulg.ac.be (author for correspondence)

KAMAL EL KADI ABDERREZZAK, Expert Researcher, (orcid.org/0000-0001-9126-1967), *EDF R&D, National Laboratory for Hydraulics and Environment (LNHE) and Saint-Venant Laboratory for Hydraulics (LHSV), Chatou, France*
Email: Kamal.El-kadi-Abderrezzak@edf.fr

SEBASTIEN ERPICUM, Assistant Professor, (orcid.org/0000-0002-7094-9604), *ArGEnCo Department, University of Liege (ULg), Research Group of Hydraulics in Environmental and Civil Engineering (HECE), Liège, Belgium*
Email: S.Erpicum@ulg.ac.be

PIERRE ARCHAMBEAU, Research Associate, (orcid.org/0000-0001-7712-3453), *ArGEnCo Department, University of Liege (ULg), Research Group of Hydraulics in Environmental and Civil Engineering (HECE), Liège, Belgium*
Email: Pierre.Archambeau@ulg.ac.be

DAMIEN VIOLEAU, Senior Scientist, (orcid.org/0000-0002-2213-5251), *EDF R&D, National Laboratory for Hydraulics and Environment (LNHE) and Saint-Venant Laboratory for Hydraulics (LHSV), Chatou, France*
Email:Damien.Violeau@edf.fr

MICHEL PIROTTON, Professor, *ArGEnCo Department, University of Liege (ULg), Research Group of Hydraulics in Environmental and Civil Engineering (HECE), Liege, Belgium*
Email: Michel.Pirotton@ulg.ac.be

BENJAMIN DEWALS, Associate Professor, (orcid.org/0000-0003-0960-1892), *ArGEnCo Department, University of Liege (ULg), Research Group of Hydraulics in Environmental and Civil Engineering (HECE), Liege, Belgium*
Email: B.Dewals@ulg.ac.be

ABSTRACT

Fluvial dikes (i.e. levees) can be damaged by overtopping flows, leading to breach formation and severe floods. Accurate prediction of the breach geometry and outflow hydrograph is crucial to achieve sound inundation risk assessment and mitigating measures. A set of laboratory experiments were performed to study overtopping induced fluvial dike breaching. The effects of floodplain tailwater on the breach expansion and outflow were investigated. Results are compared to previous experiments under different main channel inflow discharges combined with a free floodplain. The dike breaching process follows three stages: gradual start of overtopping and slow initiation of dike erosion, fast deepening and widening of the breach with highly transient flows, and flow quasi-stabilization with or without sustained breach expansion. Using the recorded data, a simplified regression model relating the breach stabilization time and the final breach width to the floodplain confinement and inflow Froude number in the main channel is proposed.

Keywords: Breach, floodplain confinement, fluvial dike, non-cohesive, overtopping, Tailwater effect.

1. INTRODUCTION

Failure of fluvial dikes (i.e. levees) often leads to devastating floods that cause loss of life and damage to public infrastructure. Understanding dike breach processes and the potential consequences of induced floods is a major concern, as sustained demographic and economic development is witnessed in dike-protected areas (Di Baldassarre et al. 2015). Frequent exposure to flow action (e.g. high or rapidly varying water levels, piping, riverside erosion), lack of maintenance, inadequate rehabilitation works and animal burrows (Orlandini et al. 2015) contribute to dike weakening and increase the risk of structural failures. Worldwide, flow overtopping (i.e. channel water level exceeding the dike crest) has been identified as the main cause of dike failure (Vorogushyn et al. 2010, Fry et al. 2012, Danka and Zhang 2015). To evaluate potential consequences of the induced floods, accurate estimates of the breach geometry and outflow are needed.

The current knowledge on fluvial dike breaching is scarce and usually transposed from studies on the breaching of embankment dams (i.e. frontal dikes) (Coleman et al 2002, Froehlich 2008, Pickert et al. 2011, Schmocker and Hager 2012, Al-Riffai 2014, Frank 2016), leading inevitably to several misconceptions. Indeed, key mechanisms of dike failure are overlooked or simplistically implemented even in detailed process-oriented models (Morris et al. 2009, ASCE/EWRI Task Committee on Dam/Levee Breaching 2011, Wahl and Lentz 2012, Danka and Zhang 2015, Peeters and al. 2016). The following points are of particular interest:

- differences in the design of fluvial dikes and embankment dams are ignored (Morris et al. 2009). The specific flow features in fluvial dike breaching are disregarded, such as the non-uniform distribution of the flow unit discharge through the breach, the parallel flow velocity along the dike and the 3D flow structures developing in the near field of the breach (Roger et al. 2009, Michelazzo et al. 2015);
- most of dike breach models, from lumped or simplified to fully discretized physically-based, rely on input parameters and empirical formulae (e.g. weir/broad-crested weir equation for breach discharge, breach shape and expansion rate) that were mainly tested for dam breach cases (Mohamed et al. 2002, Paquier and Beraud 2010, Wu 2016). The breach expansion is simulated using sediment transport capacity or erosion rate equations. These empirical equations were, however, developed for relatively low bed shear stresses, small to mild bed slopes and uniform

flows (Wu, 2016). Their applicability to dike breaching remains questionable, especially in the first phase characterized by relatively steep slopes and large flow velocity (Visser 1994).

The complexity of a dike failure model does not guarantee its accuracy, because processes described in detail are interspersed with others coarsely represented (e.g. breach widening). This lack of knowledge specific to fluvial dike failure tends to compromise both flood risk assessment and optimization of mitigating solutions. So far, several experimental studies, mainly on dam failure, have provided a sound depiction of the influence of various parameters, such as reservoir shape, dike geometry, dike material and reinforcements (e.g. Coleman 2002, Powledge et al. 1989, Pickert et al. 2011, Zhu et al. 2011, Frank and Hager 2016) or the erosion patterns at the initiation of overtopping (Kamalzare et al., 2016). In contrast, experiments on fluvial dike remain scarce and discrepancy in the results persists (Rifai et al. 2016a), while there is a pressing need for testing fluvial dike breach models against reliable datasets. Rifai et al. (2017) reviewed laboratory experiments on fluvial dike breaching and showed that, despite some recent progress, more research efforts are required to grasp the effects of various factors. While Rifai et al. (2017) examined the effects of inflow discharge and downstream boundary condition on fluvial dike breaching, no experimental study was devoted to the effects of floodplain tailwater (i.e. presence of water in the floodplain or leveed area prior to dike breaching). The tailwater effect may result typically from the increase in the floodplain water level during dike breaching or in the case of successive dike breaches. The floodplain tailwater is expected to limit strongly the breach outflow discharge and subsequently the breach expansion (Risher and Gibson 2016).

In this work, we present original laboratory experiments that investigated the floodplain backwater effects on overtopping-induced breaching of homogeneous, non-cohesive fluvial dikes. A well-documented and reliable dataset was recorded, including 3D monitoring of the breach geometry. The present set of experiments is not a scaled representation of a specific field dike. The simplification of the experimental model to a homogeneous non-cohesive dike was motivated by the ease of conducting tests, repeatability and allowed for observation of gradual evolution of the breach. The dike was, indeed, highly erodible and quickly doomed to breach upon overtopping. Literature review, presented in Rifai et al. (2017), shows that this work is at the state of the art, as recent experiments were conducted with homogenous non-cohesive dike filling (Islam, 2012, Michalazzo, 2014, Bhattarai et al., 2015, and Elalfy, 2015).

The dike was, indeed, highly erodible and quickly doomed to breach upon overtopping. The paper is organized as follows: in Section 2, a description of the experimental setup, measurements and test program is given. In Section 3, results for tests conducted with floodplain confinement are presented and compared to previous experiments with a free floodplain. A dimensional analysis for the breach widening is presented and additional key parameters to be investigated are outlined in Section 4. Conclusions are drawn in Section 5.

2. EXPERIMENTAL FACILITY

2.1. General Setup

The experiments were conducted at the Engineering Hydraulics Laboratory of the University of Liège, Belgium. The experimental facility consisted of a rectangular horizontal channel, 10 m long and l_{mc} = 1 m wide, with a 3 m long side opening toward a 4.3 m × 2.5 m floodplain (Fig. 1). The main channel and floodplain were at the same level. The opening side was obstructed with sand to represent a fluvial dike, L_d = 3 m long, h_d = 0.3 m high and of trapezoidal shape. The dike crest was l_{dc} = 0.1 m wide and the inner and outer dike face slopes were $S_i = S_o$ = 1: 2 (V:H). The sand was uniform, with a median diameter d_{50} = 1 mm and a sorting coefficient $\sigma = (d_{84}/d_{50} + d_{50}/d_{16})/2 = 1.2$, a density ρ_s = 2500 kg/m^3, a bulk density ρ_b = 1600 kg/m^3 and a porosity p = 0.36. The dike material was compacted manually, considered as constant compactive effort. Several material samples were taken from the constructed dike and analyzed. The water content was about 5.6%. Jet Erosion Tests (JET) were performed, yielding a critical shear stress τ_{cr} of 11.9 N/m^2 and an erodibility coefficient k_d of 174.5 cm^3/N/s. To trigger overtopping, a 0.02 m deep, 0.1 m wide initial notch was cut in the crest at 0.8 m from the upstream end of the dike (Fig. 1). The initial notch location and dimensions were fixed for all the experiments for the sake of repeatability and comparison of breach sections. In some tests, the flow through the breach was discharged freely from the floodplain without any storage change nor tailwater effects. In other tests, a wood panel (i.e. confinement) was added to represent floodplain inducing tailwater effects.

The discharge Q_i into the inlet basin was kept constant during each test. Honeycomb straighteners suppress surface waves, reduce turbulence and insure flow uniformity at the channel inlet. To ensure the

dike stability prior to overtopping, the seepage flow Q_d through the dike was limited by installing a drainage system at the dike bottom. The drainage system consisted of a 4 cm-thick layer of dike material wrapped in a geotextile and placed on a coarse grid. The seepage flow was collected in a reservoir located below the dike (Fig. 1). A weir (i.e. perforated plate) at the downstream end regulated the flow so that, for a given inflow discharge Q_i, the water level in the main channel was initially at the dike crest level. However, once the dike was breached the water level in the main channel did not remain constant; the tests were thus performed under falling water level conditions. Downstream of the perforated plate, water was collected in a small reservoir, at the outlet of which a V-notch weir was placed to measure the outflow discharge Q_o. For additional details, readers may refer to Rifai et al. (2017b).

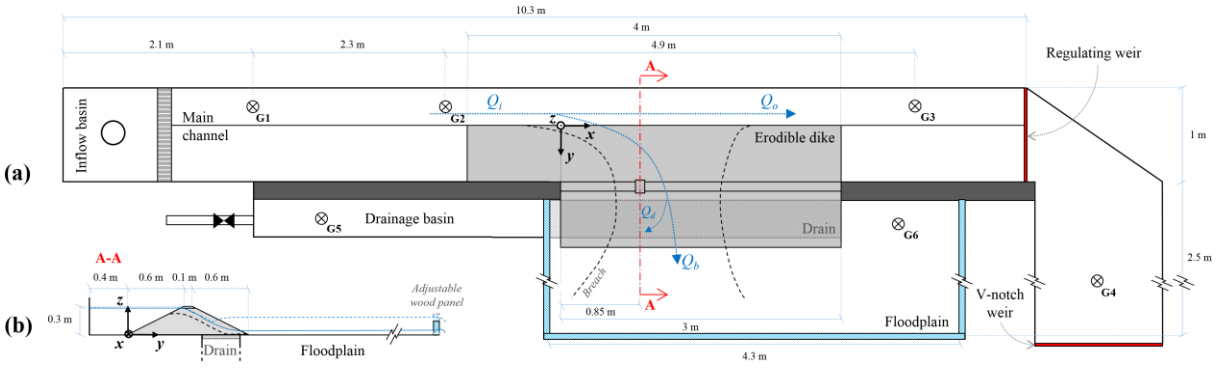

Figure 1. Laboratory setup: (a) schematic plan view, and (b) dike cross-sectional profile. The vertical reference level is at the main channel bed

2.2. Measurements

Ultrasonic distant sensors continuously measured water levels at three gauges in the main channel (G1, G2, and G3 in Fig. 1), upstream of the V-notch weir (G4), in the drainage basin (G5), and in the floodplain (G6). An electromagnetic flowmeter of ±0.4% accuracy measured the inflow discharge Q_i. The outflow discharge Q_o was deduced from the mass balance applied to a control volume located between the regulating weir (perforated plate) and the V-notch weir. The flow discharge over the V-notch weir was determined from its rating curve and water level at G4. The comparison of values with those deduced directly from the rating curve of the perforated plate shows similar results (Rifai et al., 2016). The seepage discharge Q_d was deduced from the variation of water level at G5 in the drainage tank. The breach discharge Q_b was computed based on the mass balance in the main channel, as detailed in Rifai et al. (2017).

The breach evolution was monitored by a non-intrusive laser profilometry technique consisting of a sweeping laser plan (emitted by a laser line projector Z-Laser Z30M18S3-F-640-LP75) over the whole dike. The recording was performed by a digital camera set on 1920×1080 pixels resolution, at a speed of 60 frames/s. The reconstruction system used the Direct Linear Transformation algorithm for camera calibration accounting for optical and decentering distortion (Abdel-aziz and Karara 1971). The video frames were then filtered and the 2D image coordinates of each deformed laser profile incident on the dike were transformed into 3D object coordinates. One dike sweeping enabled harvesting about ninety laser profiles, allowing the building of a detailed 3D referenced point cloud of the dike. The dike was partially under water, but bias due to refraction were corrected using the Snell-Descartes law (Glassner 1989). Further details on the geometry reconstruction are given by Rifai et al. (2016b).

2.3. Test program

The inflow discharge Q_i was set at around 0.040 m^3/s and the water level in the floodplain Z_{fp} was varied from 0.05 m to 0.20 m (Tests 1 to 6 in Table 1). These tests are compared to tests performed without floodplain confinement (Tests 7 to 20), previously analyzed by Rifai et al. (2017). The test procedure involved two steps. First, the main channel was filled progressively with a flow discharge $Q_{i0} \approx 0.75 \times Q_i$ to check the dike stability prior to overtopping. For confined floodplain tests, the elevation of the wood panel crest was first adjusted to meet the desired water level Z_{fp} in the floodplain. Then, the floodplain was filled slowly with water until reaching the level Z_{fp}. During the dike breaching, the water level in the floodplain was continuously monitored at G6 and remained roughly at the desired level; Z_{fp} almost did not change do to the breach outflow discharge. In the second step, the channel inflow discharge was increased up to Q_i. The water level increased in the main channel and the breach was triggered when the water surface exceeded the initial notch bottom.

Table 1. Test program. Tests 7 to 20 were analyzed by Rifai et al. (2017) and are used here for comparison purpose.

Test n°	Inlet Flow discharge Q_i (m^3/s)	Inlet initial Froude Number $\mathbf{F}_i$	Water level in the floodplain Z_{fp} (m)
1	0.041	0.136	0.05
2	0.040	0.133	0.10
3	0.041	0.136	0.15
4	0.041	0.136	0.15
5	0.041	0.136	0.20
6	0.041	0.136	0.20
7	0.020	0.066	0
8	0.021	0.070	

9	0.028	0.093	(free floodplain)
10	0.030	0.100	
11	0.031	0.103	
12	0.040	0.133	
13	0.040	0.133	
14	0.040	0.133	
15	0.041	0.136	
16	0.047	0.156	
17	0.050	0.166	
18	0.051	0.169	
19	0.055	0.182	
20	0.057	0.189	

Underlined test numbers refer to tests for which breach stabilization (or quasi-stabilization) was observed.

3. GENERAL RESULTS

The initial time is set when the water level in the main channel reaches the floodplain-side of the initial notch (x = 0.8 to 0.9 m and y = 0.74 m in Fig. 1a). The description of the breaching process presented hereafter is qualitatively valid for all laboratory experiments listed in Table 1. For the sake of brevity, results are shown for selected tests.

3.1. Breach evolution stages

Figure 2 shows longitudinal dike profiles at different times for Tests 3 and 14. The dike breach process can be subdivided into three main stages:

- At the early stage (Stage 0 - Initiation, blue profiles in Fig. 2) the initial notch expansion is relatively slow because the overtopping flow depth and velocity remain low. Only a slight deepening is noted, inducing an increase in the local overtopping flow depth. Stage 0 depends highly on the main channel dimensions, boundary conditions, initial notch dimensions, and on the water filling maneuvers to initiate overtopping. These parameters were not varied in the tests and measurement accuracy did not allow for an extensive study of Stage 0. Effects of Stage 0 are expected to be confined for determining the end time t_0 of the stage. The breach dimensions at time t_0 are therefore assumed similar between the tests.
- As the overtopping flow depth and velocity become larger (Stage 1 - Deepening and widening, red profiles in Fig. 2), both breach deepening and widening are promoted with a shift of the breach centerline toward the channel downstream end. The breach expansion is relatively fast because the decrease in the channel water level is slower than the breach

deepening, which results in large overtopping flow depths. The breach sides collapse gradually. The asymmetrical breach shape reflects the significant influence of flow momentum parallel to the dike crest (Rifai et al. 2017).

- In the last stage (Stage 2 - Widening, green profiles in Fig. 2), the channel free surface decreases and the flow depth starts stabilizing at its minimal level (approaching the main channel critical flow depth). The breach development becomes slower, the upstream part of the breach stops evolving, and breach deepening becomes moderate while tending to stabilize. The breach widens along the channel flow direction due to side slope failures. The breach deepening is restricted in tests with limited floodplain confinement because the non-erodible channel bottom is reached. At this stage, abrupt changes in the breach side slope can be observed at locations that coincide closely with the water level.

The transition between these three stages is not clear-cut but gradual. Nonetheless, one can highlight the main physical processes controlling each stage:

- Stage 0 is marked by slow erosion with practically constant channel flow velocity and slightly varying water levels.
- Stage 1 is characterized by breach expansion under strongly varying channel water levels and flow velocities (increasing upstream and decreasing downstream).
- Finally, Stage 2 takes place as the breach evolution is driven mainly by the strong main channel flow momentum under (quasi-) stabilized free surface and velocity.

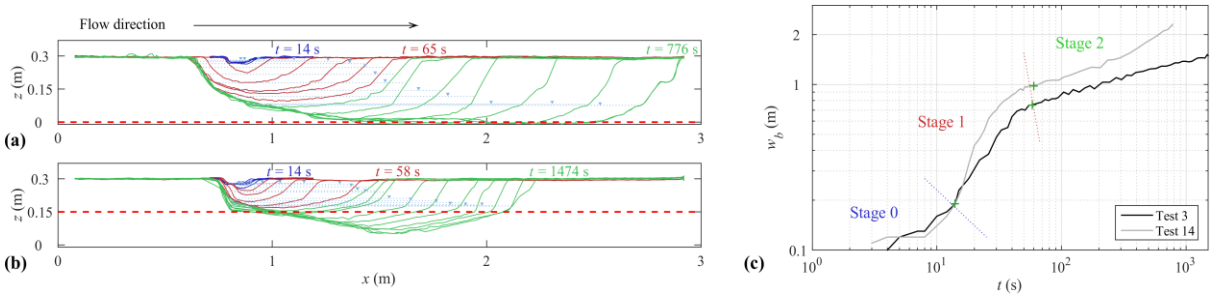

Figure 2. Longitudinal profiles at dike crest for (a) Test 3 and (b) Test 14. (····) indicate main channel average water levels. (- - -) indicate water level in the floodplain Z_{fp}. Three stages can be identified: (—) Stage 0 - Initiation, (—) Stage 1 - Deepening and widening, and (—) Stage 3 - Widening. (c) Temporal evolution of breach width w_b at the crest. Times shown in (a) and (b) indicate the time to the end of each phase

3.2. Floodplain tailwater effect on breach shape

Figure 3 shows the dike breach evolution for Tests 14, 2, and 5 corresponding to floodplain water level Z_{fp} of 0 (i.e. free floodplain), 0.1 m and 0.2 m, respectively. The breach expands much faster for a free floodplain (i.e. Test 14) because flow velocities through the breach remain high and the floodplain side of the dike is entirely exposed to high shear stresses. During Stage 0 and at the beginning of Stage 1, the breach invert did not reach the floodplain water level, thus no significant difference in the breach evolution was noted between the free floodplain test and the confined ones. Once the breach invert level becomes lower than the water level in the floodplain, the breach expansion is slowed down due to the tailwater effect reducing the energy gradient and flow velocity through the breach. Higher flow depths at the dike toe on the floodplain side cause the breach flow fan to spread and a reduction of velocity and sediment deposition at the dike plain toe (Fig. 3k and l). The side slopes of the deposition fan is about 32°, which compares well with the measured friction angle for dry sand (28° to 33°).

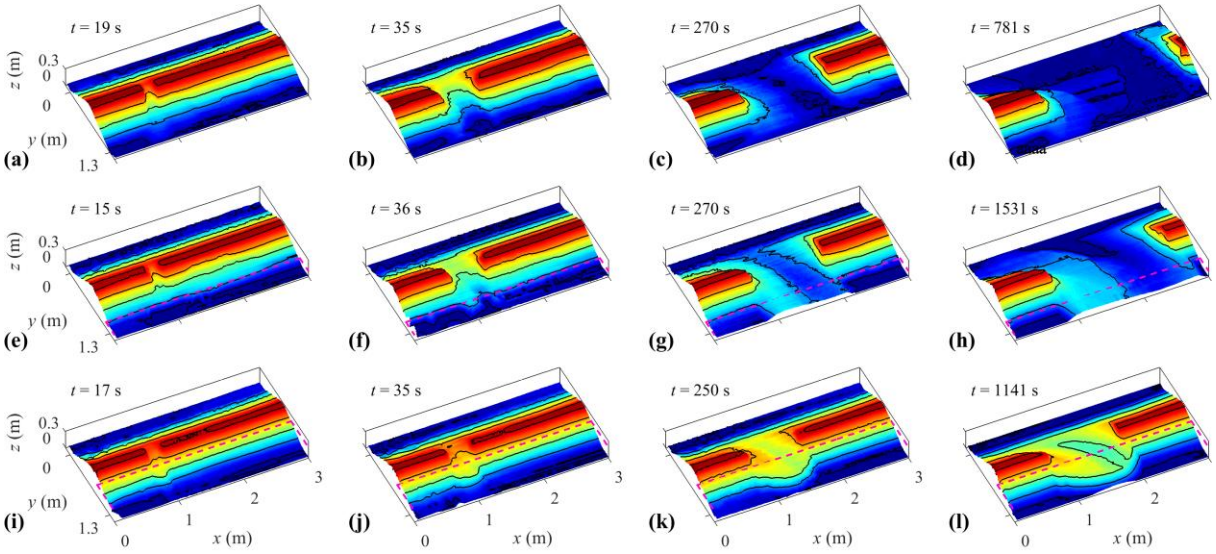

Figure 3. Breach evolution for Test 14 (a to d), Test 2 (e to h), and Test 5 (i to l). (- - -) indicates water level in the floodplain

Increasing Z_{fp} induces slower breach development and dimensions (Fig. 4). Tests for which the breach invert did not reach the main channel bottom ($Z_{fp} \geq 0.15$ m, i.e. Tests 3 to 6) show increasingly shallow breaches. The breach outflow is therefore limited (as detailed in Section 3.3). For tests with $Z_{fp} \geq 0.1$ m, the breach crest longitudinal sections show a minimum elevation point revealing the probable location of the flow maximum velocity in the breach channel (Rifai et al. 2017). The vertical offset between this minimum elevation and the water level decreases when Z_{fp} increases, indicating a decrease in the eroding

capacity of the breach outflow. Finally, the flow imprint through the breach channel is less shifted toward the downstream side of the main channel for tests with high Z_{fp} values.

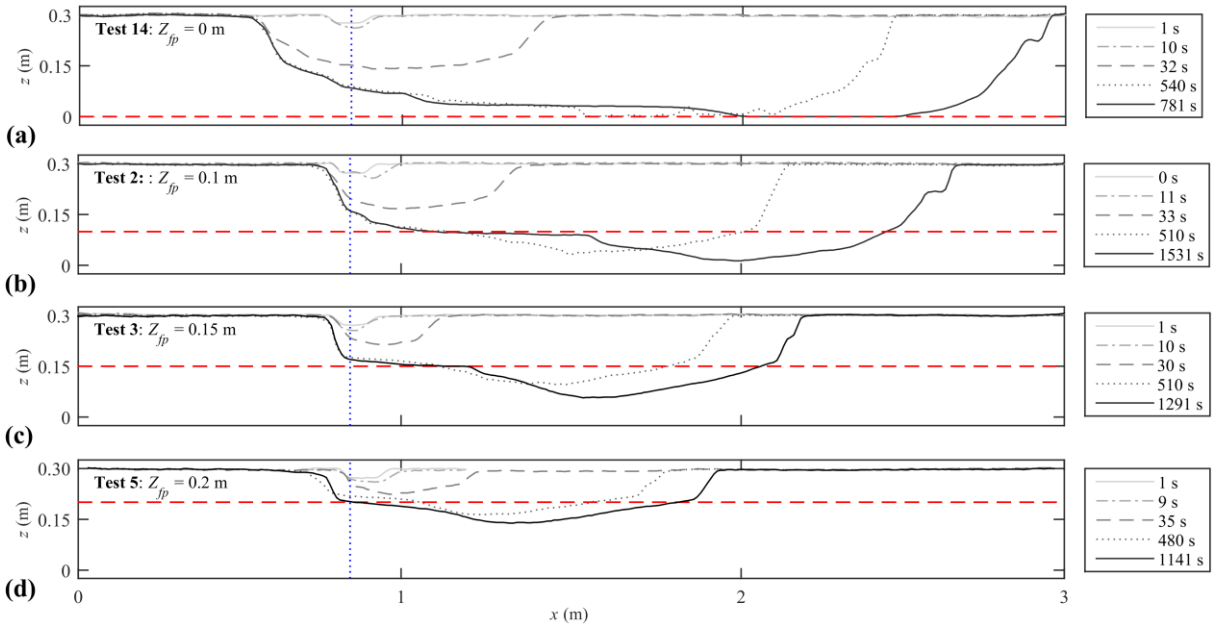

Figure 4. Longitudinal profiles at the dike crest, with (- - -) floodplain water level, (…) initial notch position

3.3. Water level and discharges

During the breaching process, the water level in the main channel z_w (computed as an average of water levels at G1, G2 and G3) decreases during the breaching process (Fig. 5a). The difference between the quasi-stabilized water level z_w and the fixed floodplain water level decreases as Z_{fp} is increased. A low floodplain confinement (i.e. Z_{fp} = 0.05 m) has almost no effect, except a limited slow-down of the hydraulic processes as the breach reaches the main channel rigid bottom. These observations recall the classical findings on the effects of weir regulation in three-branch open channel intersections (El kadi Abderrezzak et al. 2011). Higher floodplain confinements show, however, a stronger effect on the main channel water level (Fig. 5a).

Analysis of the breach discharge Q_b reveals that floodplain confinement effects are apparent once the breach invert reaches Z_{fp} (Fig. 5b); the breach expansion is slowed down (Figs. 4 and 5c) and Q_b stabilizes to lower values than in free floodplain tests. The higher the floodplain confinement, the earlier the deviation of the breach hydrograph compared to free floodplain cases (e.g. Test 14). The difference between the main channel Froude numbers upstream ($\mathbf{F}_u = [l_{mc}Q_i^2/(gA_{mc}^3]^{0.5}$, with A_{mc} as the cross-sectional main channel flow area and g the gravity acceleration) and downstream ($\mathbf{F}_d = [l_{mc}Q_o^2/(gA_{mc}^3]^{0.5}$) of the breach is strongly reduced for higher Z_{fp} values (Fig. 5d). For $Z_{fp} \geq 0.10$ m, the main channel flow

regime remains fully subcritical. For $Z_{fp} \leq 0.05$ m, $\mathbf{F}_u$ increases rapidly to reach a plateau close to 1; a shallow undulating hydraulic jump is observed upstream of the breach.

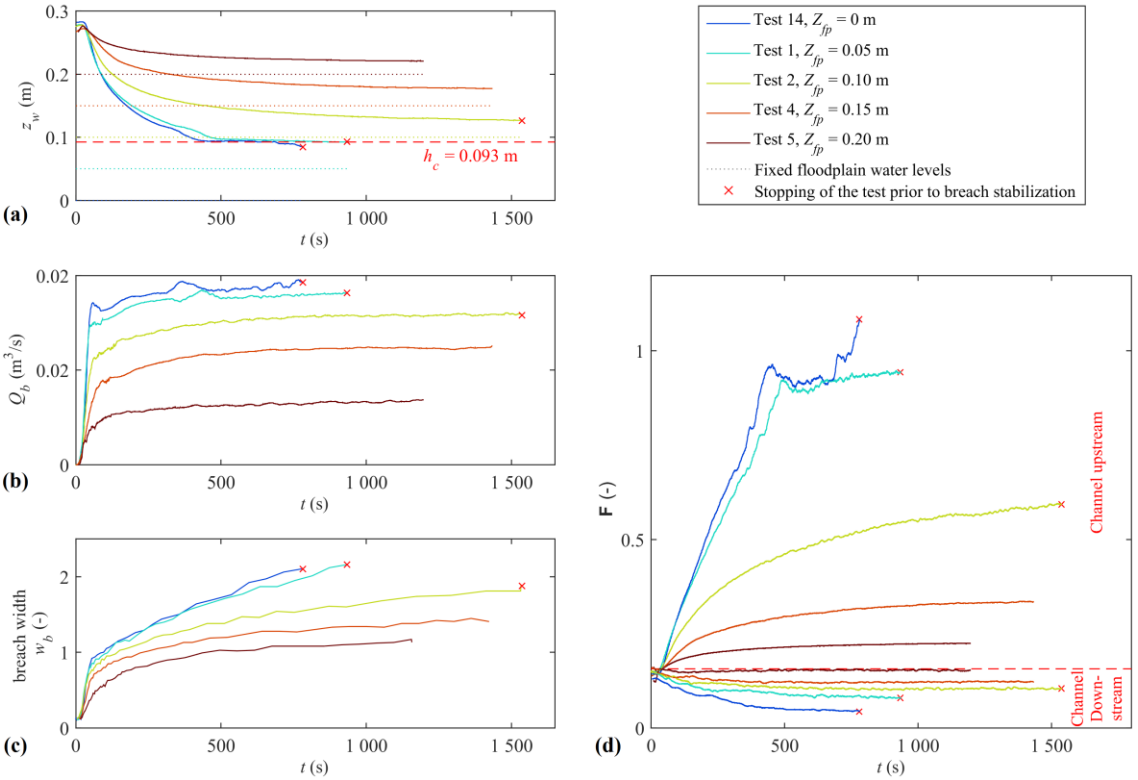

Figure 5. Time series of (a) main channel water level z_w, (b) breach discharge Q_b, (c) breach width w_b, and (d) channel upstream and downstream Froude numbers. h_c is the critical flow depth for Q_i = 0.040 m^3/s. (×) indicates test ending times because the breach reached the limits of the measuring window

3.4. Breach channel

Figure 6 shows the final breach orientation for different values of Z_{fp}. Detection of the lowest points of the breach longitudinal profiles (red and yellow lines in Fig 6), z_b, are considered as a proxy for the main flow direction in the breach channel. For all tests, the breach orientation starts almost perpendicular to the main channel and gradually rotates toward the downstream side. Tests with low (e.g. Test 1 with Z_{fp} = 0.05 m) or no floodplain confinement show a significant shift of the breach centerline toward downstream of the main channel, whereas high floodplain water levels reduce this shift (e.g. Test 5 with Z_{fp} = 0.20 m) due to the decreased breach downward widening. This observation may be related to the influence of the competition between the flow outlets (i.e. breach and downstream main channel) on the breach expansion. For $Z_{fp} \leq 0.05$ m, the main channel flow depth drops to the critical depth causing high velocities upstream of the breach, thereby generating high flow momentum and strong breach widening that results mainly from successive slope collapses of the breach downstream side. In contrast,

increasing the floodplain confinement (i.e. $Z_{fp} \geq 0.15$ m) limits the drop of the main channel water level; the breach slowly widens and gradually deviates to accommodate the breach outflow.

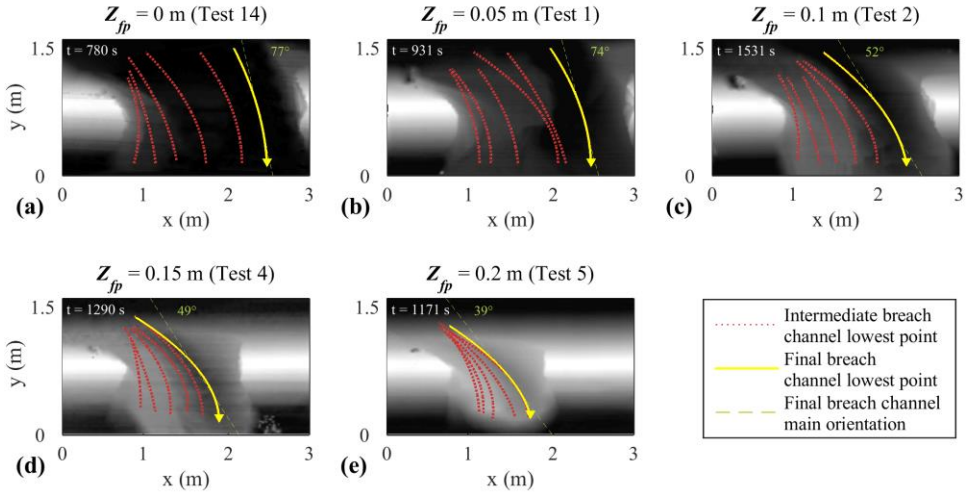

Figure 6. Final breach channel orientation for different floodplain confinement conditions

In contrast to free or low floodplain confinement tests ($Z_{fp} \leq 0.05$ m), for which the breach invert reaches the main channel rigid bottom, tests with $Z_{fp} \geq 0.10$ m enable the observation of non-constraint breach deepening like the case of dike breaching with erodible main channel and floodplain beds (Islam 2012, Michelazzo 2014, Kakinuma et al. 2014). In this case, the flow remains more concentrated in the centerline of the breach channel, limiting therefore the breach widening as less shear stresses are exerted on the breach channel downstream side. In contrast, for tests in which the channel bottom is reached, the breach flow causes more erosion on the breach channel downstream side.

4. Discussion

Fluvial dike breach evolution is controlled by two sets of parameters: (1) dike properties (geometry and composition) and (2) hydraulic loads. Tests presented in Section 3 have focused on the second set of parameters by investigating the floodplain confinement effects. In the following discussion, we include the results by Rifai et al. (2017) who investigated the effects of the main channel inflow discharge on the breach expansion.

4.1. Breach evolution

Figure 7a shows the location of upstream and downstream sides of the breach at the crest level, with the initial notch at x = 0.8 m, for various inflow discharges Q_i (Tests 7 to 20 plotted in colored lines) with a free floodplain and for $Q_i \approx 0.040$ m^3/s with different floodplain confinements Z_{fp} (Tests 1 to 6 and Test

14 illustrated by black lines with symbols). The breach maximal width $w_{b,max}$ is defined as the distance between the breach sides. The three stages defined in Section 3.1 are visible, especially the breach downward widening (Fig. 7a). The breach lowest point deepening confirms the previous phasing of the breach evolution (Fig. 7b). For the breach widening, significant differences in-between the tests are apparent during Stages 1 and 2. In all the tests, no definite stabilization of the breach width was observed. Nonetheless, we consider the breach width is "quasi-stabilized" at the end of the tests with $Z_{fp} \geq 0.15$ m (i.e. Tests 3 to 6) or $Q_i \leq 0.021$ m^3/s (i.e. Tests 7 and 8). The strong dependency of the breach downward widening on Q_i and Z_{fp} is clearly illustrated by Fig. 7a. The upward widening occurs only during Stages 0 and 1. The stabilized downward width decreases with increasing floodplain confinements. This can be attributed to low flow velocities upstream of the main channel for higher Z_{fp}, thus generating weak erosion of the dike internal face. Tests with free floodplain and $Q_i > 0.050$ m^3/s show similar continuing and strong downward breach widening during Stages 1 and 2.

From Fig. 7b, no clear dependency of the lowest breach point to the inflow discharge can be deduced, as the breach reaches the non-erodible bottom of the flume for tests with various Q_i. The offset between the lowest point of the quasi-stabilized breach and the floodplain water level Z_{fp} tends to increase with decreasing Z_{fp} for tests that did not reach the flume non-erodible bottom (i.e. Tests 3 to 6). This indicates that, for free floodplain configurations, strong breach flow inducing high shear stresses would promote stronger erosion of the main channel and/or floodplain bottoms if these later were made of erodible material (Islam 2012, Kakinuma 2013, Michelazzo 2014).

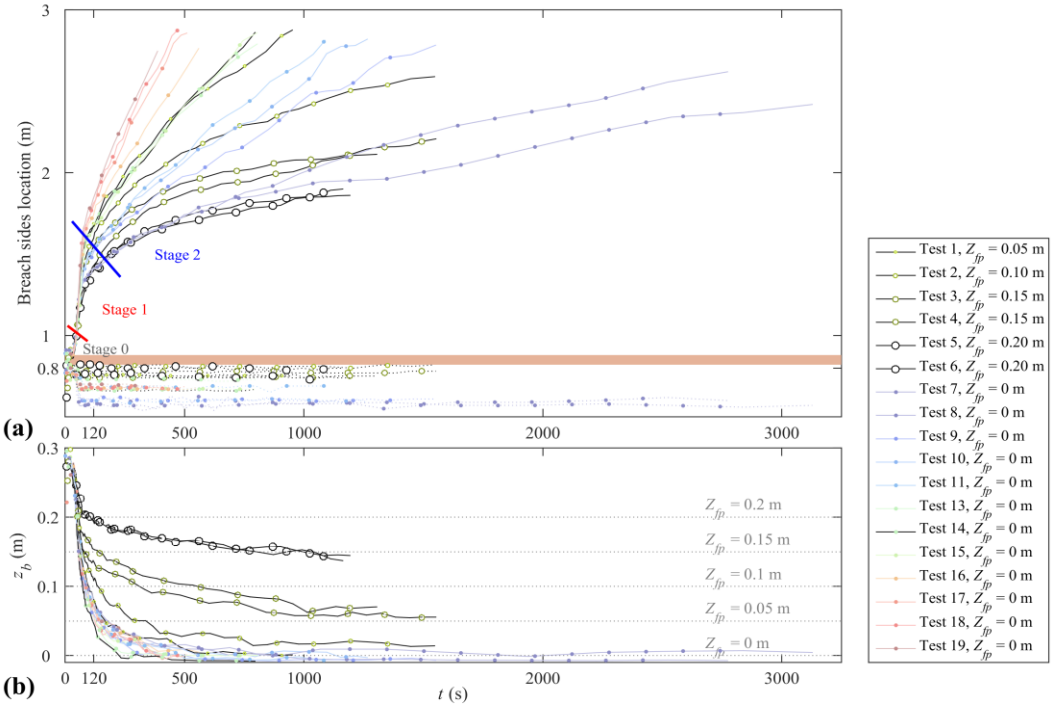

Figure 7. (a) Temporal up- and downstream breach widening, with initial notch at x = 0.8 m; (b) temporal development of lowest point in the breach cross section

4.2. Breach quasi-stabilization

We note from Sections 3.3 (Fig. 5) and 4.1 (Fig. 7) that breach stabilization (or quasi-stabilization) occurs during Stage 2, under already stabilized flow conditions. Therefore, for characterizing the breach stabilization, we focus here only on Stages 1 and 2. We define a dimensionless breach width $w_b^* = w_b/h_d$, which can be expressed as a function of:

- the dimensionless time $t^* = (t - t_0)g'^{1/2}h_c h_d^{-1}d_{50}^{-1/2}$, as defined by Schmocker and Hager (2012).
- the initial Froude number in the main channel $\mathbf{F}_i = [l_{mc}Q_i^2/(gA_{mc}^3)]^{1/2}$.
- and the dimensionless floodplain confinement $Z_{fp}^* = Z_{fp}/h_d$.

where t_0 is the beginning time of Stage 1, $g' = g[(\rho_s - \rho)/\rho]$ is the submerged specific gravity with ρ as the water density. The dimensionless width w_b^* can be modeled by the following power law, retained for all tests with and without floodplain backwater effects (Fig. 8):

$$w_b^* = \alpha t^{*\beta} \tag{1}$$

where the coefficient α and exposure β are assumed $\mathbf{F_i}$ and Z_{fp}^* dependent. Using regression analysis on the data of Stage 2, the following relationships are found:

$$\alpha = 0.02\mathbf{F}_i^{-1.1}, \text{ and } \beta = 0.9\mathbf{F}_i^{0.46}(1 - Z_{fp}^*)^{0.21} \tag{2}$$

The agreement between the adjusted model and measurements is deemed satisfactory as the determination coefficient R^2 remains above 0.75 (Fig. 8c). During Stage 1, moderate deviations are noted (Fig. 9), with the breach widening being underestimated. This may be attributed to stronger breach widening during Stage 1 that was promoted by high overtopping flow depths and emptying of the main channel. In that respect, dynamics and fluctuations of the overtopping flow depth and velocity are highly dependent on the main channel dimensions that were not varied in the tests. Therefore, breach evolution during Stages 1 and 2 is modeled with Eq. (1) while effects of specific increments of Stage 1 are ignored. The breach width is overestimated during Stage 2 for Tests 7 and 8 (corresponding to the lowest inflow discharge $Q_i \approx 0.02$ m^3/s). For these tests, the breach widens by successive collapses of the downstream side slopes, which are held by negative pore pressure of the unsaturated soil matrix (Pickert et al. 2011, Rifai et al. 2017). Therefore, effects of apparent cohesion are suspected to be prominent under relatively low shear stresses due to low flow velocities in Tests 7 and 8. The breach width is underestimated by Eq. (1) for Tests 5 and 6 conduced with the highest floodplain confinement (i.e. $Z_{fp} = 0.20$ m).

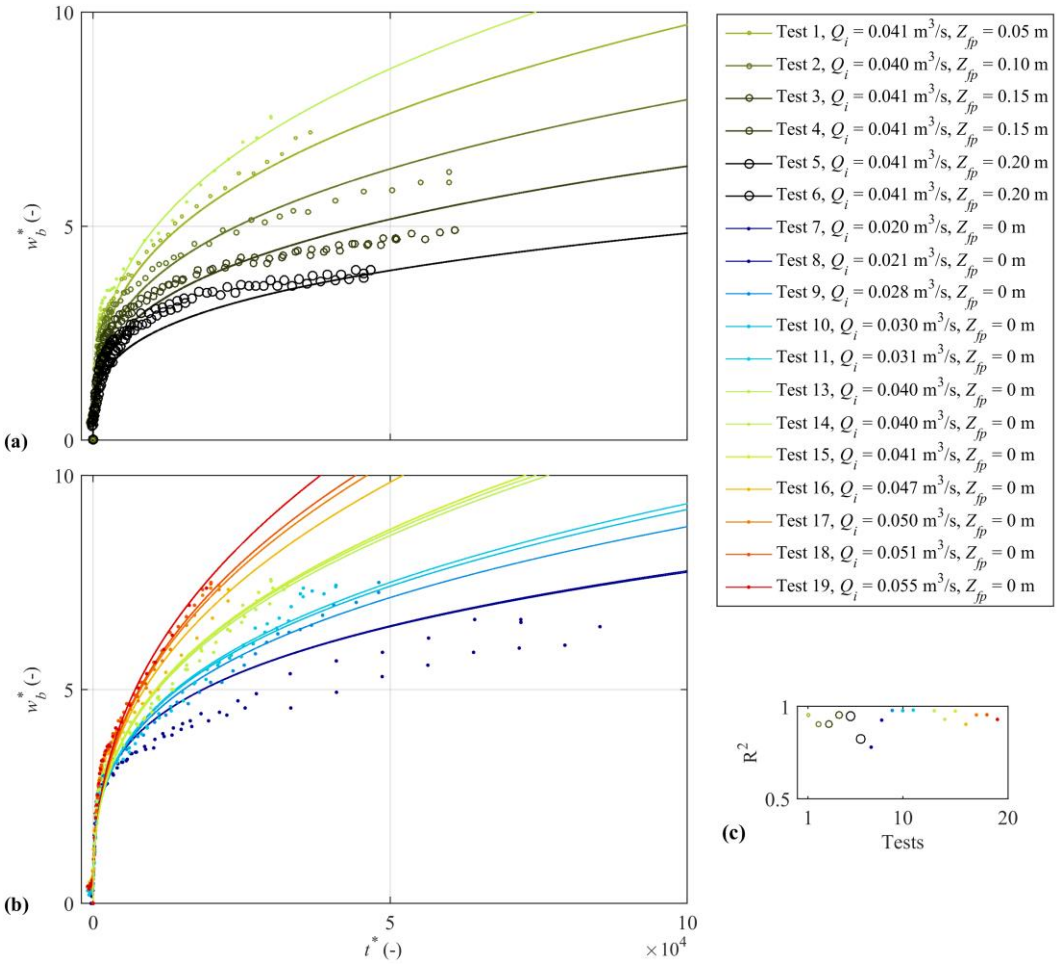

Figure 8. Dimensionless breach width *vs* dimensionless time for (a) tests with varying confinement levels and inflow discharge of 0.040 m^3/s, and for (b) tests with varying inflow discharges combined with a free floodplain. (c) Determination coefficients.

Tests 5 and 6 are considered as quasi stabilized and the dimensionless breach widening velocity at the end of each test is $v_{b,eq}^* = dw_b^*/dt^* = \alpha\beta t^{*(\beta-1)} \approx 2 \times 10^{-5}$. Using this stability criterion, the dimensionless stabilized breach width $w_{b,eq}^*$ and the dimensionless stabilization time t_{eq}^* for the remaining tests are estimated as (Fig. 10):

$$t_{eq}^* = [v_{b,eq}^* / (\alpha\beta)]^{1/(\beta-1)} \quad (3)$$

$$w_{b,eq}^* = \alpha[v_{b,eq}^* / (\alpha\beta)]^{\beta/(\beta-1)} \quad (4)$$

The computed dimensionless final breach width ranges from $w_{b,eq}^* = 4.2$ for Tests 5 and 6 to $w_{b,eq}^* = 32$ for Test 19. The computed dimensionless stabilization time ranges from $t_{eq}^* \approx 10^{4.7}$ for Tests 5 and 6 to $t_{eq}^* \approx 10^{5.8}$ for Test 19. This corresponds to $w_{b,eq} = 1.26$ m and $t_{eq} \approx 1300$ s for Tests 5 and 6 and $w_{b,eq} = 9.6$ m and $t_{eq} \approx$ 3h40 min for Test 19. For very low initial Froude numbers and strong level of confinement (left had side of gray dashed lines), the performance of Eqs. (3-4) to reproduce the breach width evolution and stabilization decreases (Fig. 10).

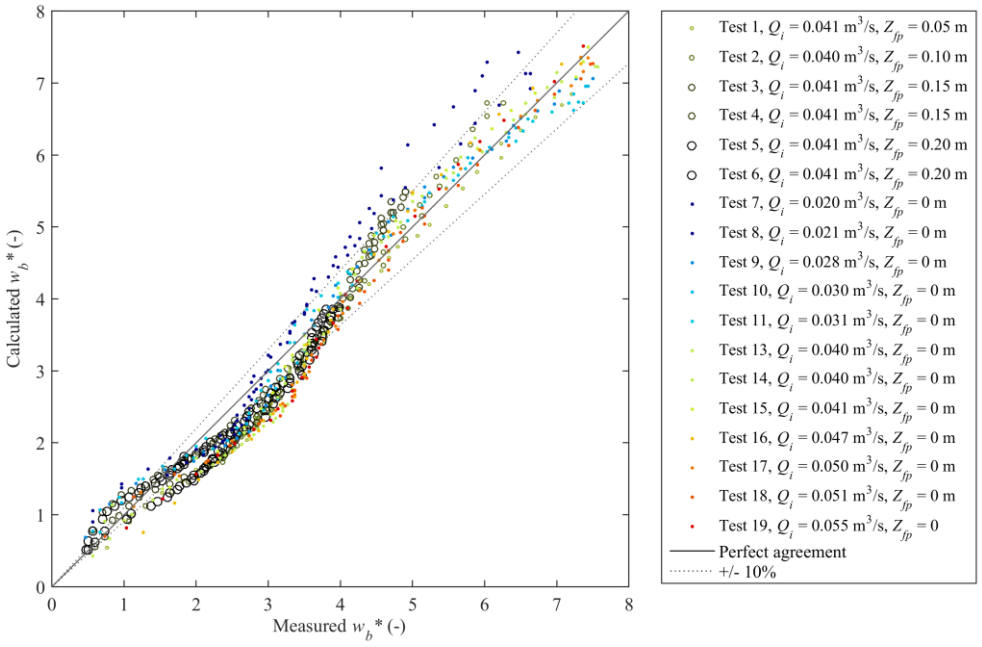

Figure 9. Comparison between measured and computed dimensionless breach widths

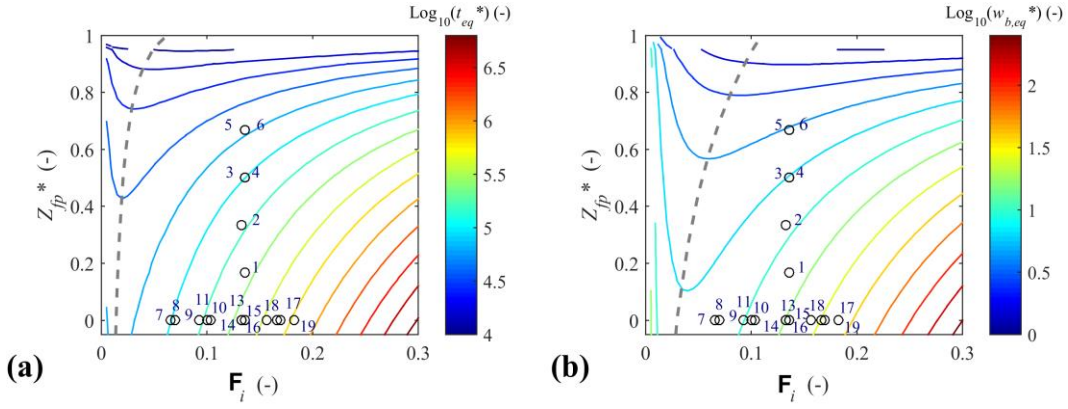

Figure 10. Breach stabilization. (a) Computed stabilization time, and (b) Stabilized width computed using $w_{b,eq}^* = 2\times10^{-5}$

4.3. Sensitivity of the breach evolution to F_i and Z_{fp}

The regression model (i.e. Eq. 1) allows estimating the breach duration and final width. However, Stage 0 was ignored and Stage 1 was not properly reproduced. The determination of t_{eq}^* and $w_{b,eq}^*$ enables the normalization of results with respect to the breach final state (Fig. 11). Figure 11 shows an overall good agreement except for Tests 5 and 6 that stand out of the rest. Tests 5 and 6 were conducted with the highest levels of floodplain confinement and the breach expansion process might be excessively altered in this case.

Tests 3 to 8 cover merely the whole breach evolution path, meaning that the breach at the end of the test is indeed stabilized. In contrast, without floodplain confinement, and for $Q_i > 0.040$ m^3/s the breach width reaches only 25 to 45 % of the estimated final width, corresponding to 3 to 12 % of the breaching time.

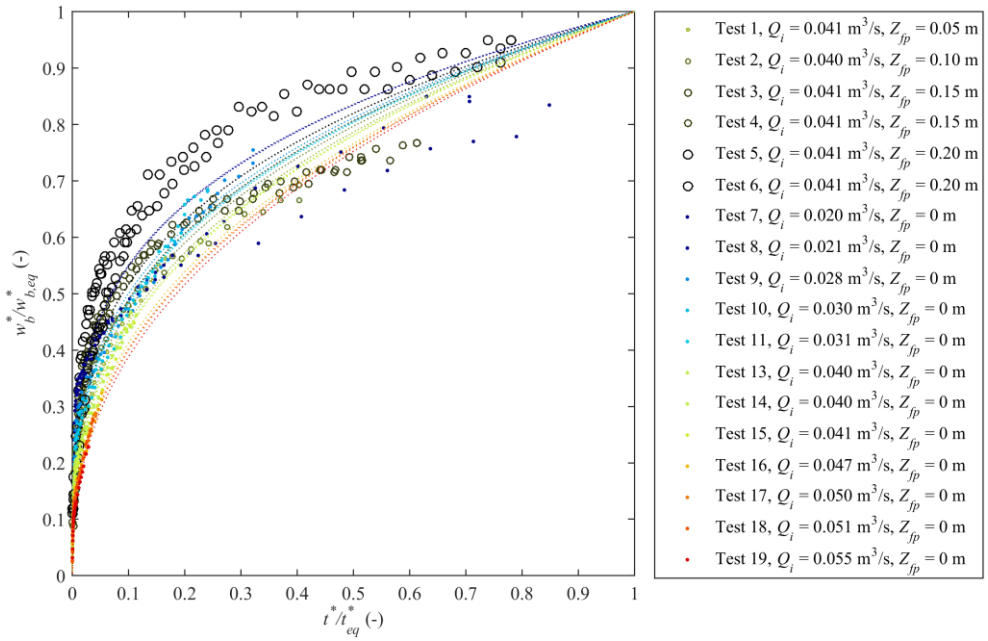

Figure 11. Normalized breach width vs. normalized time

5. Conclusion

This paper has addressed flow overtopping-induced breaching of non-cohesive homogenous fluvial dikes. A series of laboratory experiments were performed to investigate the effects of floodplain backwater (i.e. tailwater) on the breach discharge and geometry. Results were compared with previous observations on fluvial dike breaching under free floodplain conditions for a range of inflow discharges in the main channel. Combination of all datasets shed light on the relative influence of the main channel flow velocity and momentum and of the transversal flow energy line on the breach expansion.

The experimental observations highlighted three stages in the dike breaching process: gradual start of flow overtopping and slow initiation of dike erosion (Stage 0), fast breach deepening and widening with highly transient flows (Stage 1), and flow quasi-stabilization with or without sustained breach expansion (Stage 2). The reduced energy gradient through the breach channel promoted its stabilization. The deviation of the breach channel centerline was particularly affected and the shift toward downstream was considerably reduced for high levels of floodplain confinement. During Stage 2, the breach widening can be described by a formulation that relates the dimensionless breach width to a dimensionless time, the inlet Froude number and floodplain confinement level. Results revealed a high sensitivity of the stabilized breach width and duration to these two parameters. However, the proposed formulation is derived from a restricted number of experiments with the same dike composition (non-cohesive sand of 1 mm in diameter). Stage 0 was cut off from the breach evolution analysis and Stage 1 was moderately modeled by the equation.

Stages 0 and 1 remain of particular relevance and should be further analyzed. Characterization of Stage 0 is crucial to predict the dike breach triggering and to plan emergency intervention. Similarly, breach evolution during Stage 1 should be improved to reduce uncertainty in flood risk estimation in the near field of the dike, as fast increase of the breach discharge occurs during Stage 1. Finally, the effects of other parameters on the breaching processes have to be investigated, such as dike materiel and geometry, main channel geometry and inflow discharge unsteadiness. These topics are under investigation through experimental and numerical modelling.

Notation

A_{mc} = cross-sectional main channel flow area (m^2)

407 d_{50} = grain size such that 50% of the sample is finer than d_{50} (mm)

408 $\mathbf{F}_i$ = Froude number in main channel prior to overtopping (-)

409 $\mathbf{F}_u$ = Froude number in the upstream part of the channel (-)

410 $\mathbf{F}_d$ = Froude number in the downstream part of the channel (-)

411 g = gravity acceleration (m/s^2)

412 g' = submerged specific gravity (m/s^2)

413 h_d = dike height (m)

414 h_c = critical flow depth in the main channel (m)

415 k_d = Erodibility coefficient ($cm^3/N/s$)

416 l_{dc} = dike crest width (m)

417 L_d = dike length (m)

418 L_{mc} = main channel length (m)

419 l_{mc} = main channel width (m)

420 p = porosity (-)

421 Q_b = breach discharge (m^3/s)

422 Q_d = drainage discharge (m^3/s)

423 Q_i = main channel inflow discharge (m^3/s)

424 Q_{i0} = channel filing inflow discharge (m^3/s)

425 Q_o = channel outflow discharge (m^3/s)

426 S_i, S_o = dike side slopes (channel side and floodplain side respectively) (-)

427 t = time (s)

428 t^* = dimensionless time (-)

429 t_0 = time at the end of Stage 0 (i.e. time of beginning of Stage 1) (s)

430 t_{eq} = estimated breach equilibrium time (s)

431 t_{eq}^* = estimated dimensionless breach equilibrium time (-)

432 v_b^* = dimensionless breach widening velocity (-)

433 $v_{b,eq}^*$ = dimensionless stabilization breach widening velocity (-)

434 w_b = breach width (m)

435 $w_{b,max}$ breach maximal width, defined as the distance between the breach sides (m)

436 w_b* = dimensionless breach width (-)

437 $w_{b,eq}$ = estimated equilibrium breach width (m)

438 $w_{b,eq}$* = estimated dimensionless equilibrium breach width (-)

439 x = longitudinal distance (m)

440 y lateral distance (m)

441 z = elevation (m)

442 z_b = elevation of the breach lowest point (m)

443 z_w = averaged water level in the main channel (m)

444 Z_{fp} = fixed floodplain water level (m)

445 Z_{fp}* = dimensionless fixed floodplain water level (-)

446 α = coefficient (-)

447 β = exponent (-)

448 ρ = water density (kg/m^3)

449 ρ_b = bulk density (kg/m^3)

450 ρ_s = sand density (kg/m^3)

451 τ_{cr} = critical shear stress (N/m^2)

452 **References**

453 Al-Riffai, M. (2014), Experimental study of breach mechanics in overtopped non-cohesive earthen
454 embankments, PhD thesis, Univ. of Ottawa, Ottawa, Canada.
455 Abdel-aziz, I. Y., and H. M. Karara (1971), Direct linear transformation from comparator coordinates
456 into object space coordinates in close-range photogrammetry. In ASP Symposium on Close-
457 Range Photogrammetry 1971, Illinois, USA.
458 ASCE/EWRI Task Committee on Dam/Levee Breaching (2011), Earthen embankment breaching, J.
459 Hydraul. Eng., 137(12), 1549–1564.
460 Bhattarai, P. K., H. Nakagawa, K. Kawaike, and H. Zhang, (2015), Study of breach characteristics and
461 scour pattern for overtopping induced river dyke breach, paper presented at 36th IAHR World
462 Conference, The Hague, Netherlands.
463 Coleman, S. E., D. P. Andrews, and M. G. Webby (2002), Overtopping breaching of noncohesive
464 homogeneous embankments, J. Hydraul. Eng., 128(9), 829–838.
465 Danka, J., and L. M. Zhang (2015), Dike failure mechanisms and breaching parameters, J. Geotech. and
466 Geoenviron. Eng., 10.1061/(ASCE)GT.1943- 5606.0001335, 04015039.
467 Di Baldassarre, G., A. Viglione, G. Carr, L. Kuil, K. Yan, L. Brandimarte, and G. Blöschl (2015),
468 Debates-Perspectives on socio-hydrology: Capturing feedbacks between physical and social
469 processes, Water Resour. Res., 51, 4770–4781, doi:10.1002/2014WR016416.
470 Elalfy, E. Y. E. M. Numerical and experimental investigations of dam and levee failure (2015), PhD
471 thesis, Univ. of South Carolina, South Carolina, USA.
472 El kadi Abderrezzak, K., L. Lewicki, A. Paquier, N. Rivière, and G. Travin (2011), Division of critical
473 flow at three-branch open-channel intersection, J. Hydraul. Res., 49(1), 231–238,
474 doi:10.1080/00221686.2011.558174
475 Frank, P.-J. (2016), Hydraulics of spatial dike breach, PhD thesis, Univ. of Zurich, Zurich, Switzerland.
476 Frank, P.-J., and W. H. Hager (2016), Challenges of dike breach hydraulics, paper presented at the 8th
477 International Conference on Fluvial Hydraulics (River Flow), International Association for
478 Hydro-Environment Engineering and Research (IAHR), Saint Louis, Mo, USA.
479 Froehlich, D. C. (2008), Embankment dam breach parameters and their uncertainties, J. Hydraul. Eng.,
480 134(12), 1708–1721.

Fry, J., A. Vogel, P. Royet, and J.-R. Courivaud (2012), Dam failures by erosion: Lessons from ERINOH data bases, paper presented at the 6th International Conference on Scour and Erosion (ICSE), International Association for Hydro-Environment Engineering and Research (IAHR), Paris, France.

Glassner, A. S. (1989), An Introduction to Ray tracing, 328 pp., International Society for Soil Mechanics and Foundation Engineering (ISSMGE), Elsevier Sci., London.

Islam, S. (2012), Study on levee breach and successive disasters in low-land through numerical and experimental approaches, PhD thesis, Nagoya Univ., Nagoya, Japan.

Kamalzare, M., F. T. Zimmie, B. Cutler, and W. R. Franklin (2016), New Visualization Method to Evaluate Erosion Quantity and Pattern, Geotechnical Testing Journal, 39(3), 431-446.

Mohamed, M. A. A., P. G. Samuels, M. W. Morris, and G. S. Ghataora (2002), Improving the accuracy of prediction of breach formation through embankment dams and flood embankments, paper presented at the 1st International Conference on Fluvial Hydraulics (River Flow), International Association for Hydro-Environment Engineering and Research (IAHR), Louvain-la-Neuve, Belgium.

Kakinuma T., D. Tobita, H. Yokoyama, and A. Takeda (2013), Levee breach observation at Chiyoda experimental flume, paper presented at the 12th International Symposium on River Sedimentation (ISRS), IRTCES, Kyoto, Japan.

Kakinuma, T., and Y. Shimizu (2014), Large-scale experiment and numerical modeling of a riverine levee breach, J. Hydraul. Eng., 140(9), 1−9.

Michelazzo, G., H. Oumeraci, and E. Paris (2015), Laboratory study on 3D flow structures induced by zero-height side weir and implications for 1D modeling. J. Hydraul. Eng., 141(10), 4015023, doi: /10.1061/(ASCE)HY.1943-7900.0001027

Michelazzo, G. (2014). Breaching of river levees : analytical flow modelling and experimental hydro-morphodynamic investigations, PhD thesis, University of Florence, Italy.

Morris, M., M. A. A. M. Hassan, A. Kortenhaus, and P. Visser (2009), Breaching processes: A state of the art review. FLOODsite Project Report, HR Wallingford, Wallingford, UK.

508 Orlandini, S., G. Moretti, and J. D. Albertson (2015), Evidence of an emerging levee failure mechanism
509 causing disastrous floods in Italy, Water Resour. Res., 51, 7995–8011, doi:
510 10.1002/2015WR017426.
511 Paquier A. and C. Beraud, (2010), Validating a simplified model for flood hazard downstream levees,
512 paper presented at the 5th International Conference on Fluvial Hydraulics (River Flow)
513 International Association for Hydro-Environment Engineering and Research (IAHR),
514 Braunschweig, Germany.
515 Pickert, G., V. Weitbrecht, and A. Bieberstein (2011), Beaching of overtopped river embankments
516 controlled by apparent cohesion, J. Hydraul. Res., 49(2), 143–156.
517 Peeters, P., M. Heredia Gomez, M. van Damme and P. J. Visser (2016), Unveiling the consequences of
518 your breach growth model choice, paper presented at the 3rd European Conference on Flood Risk
519 Management (FLOODrisk), Lyon, France.
520 Powledge, G. R., D. C. Ralston, P. Miller, Y. H. Chen, P. E. Clopper, and D. M. Temple (1989),
521 Mechanics of overflow erosion on embankments. I: Research activities, J. Hydraul. Eng., 115(8),
522 1040 – 1055
523 Roger, S., B. J. Dewals, S. Erpicum, D. Schwanenberg, H. Schuttrumpf, J. Kongeter, and M. Pirotton
524 (2009), Experimental and numerical investigations of dike-break induced flows, J. Hydraul. Res.,
525 47(3), 349–359.
526 Rifai, I., S. Erpicum, P. Archambeau, D. Violeau, M. Pirotton, B. Dewals, and K. El Kadi Abderrezzak
527 (2016a), Sensitivity of the breaching process in the case of overtopping induced fluvial dike
528 failure, paper presented at the 8th International Conference on Fluvial Hydraulics (River Flow),
529 International Association for Hydro-Environment Engineering and Research (IAHR), Saint
530 Louis, Mo, USA.
531 Rifai, I., S. Erpicum, P. Archambeau, D. Violeau, M. Pirotton, K. El Kadi Abderrezzak, and B. Dewals
532 (2016b), Monitoring topography of laboratory fluvial dike models subjected to breaching based
533 on a laser profilometry technique, paper presented at the 13th International Symposium on River
534 Sedimentation (ISRS), IRTCES, Stuttgart, Germany.

Rifai, I., S. Erpicum, P. Archambeau, D. Violeau, M. Pirotton, K. El Kadi Abderrezzak, and B. Dewals (2017), Overtopping induced failure of noncohesive, homogeneous fluvial dikes, Water Resour. Res., 53, 3373 – 3386, doi: 10.1002/2016WR020053.

Risher, P., S. Gibson (2016), Applying Mechanistic Dam Breach Models to Historic Levee Breaches, paper presented at the 3rd European Conference on Flood Risk Management (FLOODrisk), Lyon, France.

Schmocker, L., and W. H. Hager (2012), Plane dike-breach due to overtopping: Effects of sediment, dike height and discharge, J. Hydraul. Res., 50(6), 576–586.

Visser, P. J. (1994). Application of sediment transport formulae to sand-dike breach erosion. Communications on hydraulic and geotechnical engineering, No. 1994-07, TU Delft, NL.

Vorogushyn, S., B. Merz, K. E. Lindenschmidt, and H. Apel. (2010), A new methodology for flood hazard assessment considering dike breaches, Water Resour. Res., 46, W08541, doi:10.1029/2009WR008475.

Wahl, T., and D. Lentz (2012), Experimental methods for studying canal breach processes, paper presented at the 4th Hydraulic Measurements and Experimental Methods Conference (HMEM), American Society of Civil Engineers (ASCE) - Environmental and Water Resources Institute (EWRI), Snowbird, Utah, USA.

Wu, W. (2016), Introduction to DLBreach - A simplified physically-based dam/levee breach model. Technical Report, Department of Civil and Environmental Engineering, Clarkson University, NY, USA.

Zhu, Y., P. J. Visser, J. K. Vrijling, and G. Wang (2011), Experimental investigation on breaching of embankments, Sci. China, Ser. E: Technol. Sci., 54(1), 148–155.